



Published in final edited form as:

Bone. 2024 July ; 184: 117106. doi:10.1016/j.bone.2024.117106.

Combining Anabolic Loading and Raloxifene Improves Bone Quantity and Some Quality Measures in a Mouse Model of Osteogenesis Imperfecta

Amy Creecy¹, Dyann Segvich¹, Corinne Metzger², Rachel Kohler¹, Joseph M. Wallace¹

¹Department of Biomedical Engineering, Indiana University Purdue University Indianapolis

²Department of Anatomy, Cell Biology, and Physiology, Indiana University School of Medicine Indianapolis, IN

Abstract

Osteogenesis imperfecta (OI) increases fracture risk due to changes in bone quantity and quality caused by mutations in collagen and its processing proteins. Current therapeutics improve bone quantity, but do not treat the underlying quality deficiencies. Male and female G610C+/- mice, a murine model of OI, were treated with a combination of raloxifene and in vivo axial tibial compressive loading starting at 10 weeks of age and continuing for 6 weeks to improve bone quantity and quality. Bone geometry and mechanical properties were measured to determine whole bone and tissue-level material properties. Colocalized Raman/nanoindentation system was used to measure chemical composition and nanomechanical properties in newly formed bone compared to old bone to determine if bone formed during the treatment regimen differed in quality compared to bone formed prior to treatment. Lastly, lacunar geometry and osteocyte apoptosis were assessed. OI mice were able to build bone in response to the loading, but this response was less robust than in control mice. Raloxifene improved some bone material properties in female but not male OI mice. Raloxifene did not alter nanomechanical properties, but loading did. Lacunar geometry was largely unchanged with raloxifene and loading. However, osteocyte apoptosis was increased with loading in raloxifene treated female mice. Overall, combination treatment with raloxifene and loading resulted in positive but subtle changes to bone quality.

Keywords

osteogenesis imperfecta; mechanical loading; raloxifene; bone quality

Corresponding author: Amy Creecy, MS 543, 635 Barnhill Dr, Indianapolis, IN 46202, acreecy@iu.edu.

Declarations of interest: none

Publisher's Disclaimer: This is a PDF file of an unedited manuscript that has been accepted for publication. As a service to our customers we are providing this early version of the manuscript. The manuscript will undergo copyediting, typesetting, and review of the resulting proof before it is published in its final form. Please note that during the production process errors may be discovered which could affect the content, and all legal disclaimers that apply to the journal pertain.

1. Introduction

Osteogenesis imperfecta (OI) is a condition of poor bone quality caused by mutations in collagen and its processing proteins that result in skeletal fragility due to deficiencies in structure such as cortical thinning and poor quality of bone [1]. Bone tissue quality changes include hypermineralization, collagen fibrillar defects, and high lacunar density [2–5]. The standard of care for OI is to treat with bisphosphonates, which have been repurposed from use in osteoporosis [6]. These medications improve the quantity of bone but do alter the quality. Improving the quantity of poor-quality material will have limited benefits on preserving skeletal mechanical integrity. Preclinical and early clinical research have started to address this issue, with studies examining the benefits of anti-sclerostin antibody, anti-TGF- β antibody, or targeting cellular stress [7–12] on bone quality. However, combining treatments that improve quantity and quality will be necessary due to the structural and quality deficiencies present in OI.

Raloxifene (RAL) is one therapeutic that could potentially improve bone quality. RAL is a selective estrogen receptor modulator (SERM) that has been approved to prevent vertebral fractures in post-menopausal women [13]. SERMs may affect tissues differently based on which estrogen receptor (ER) (α or β) they bind to and whether heterodimerization or homodimerization occurs [14]. Additionally, males and females respond differently to estrogen and therefore SERMs [15]. While raloxifene may promote bone formation [14], it has also been shown to improve bone quality in a cell-independent manner [16–18]. Previous work in the lab has shown that treatment of a severe model of OI with RAL resulted in OI mice having fewer spontaneous fractures [19]. This improvement may be due to RAL increasing the bound water content of bone thereby improving bone quality and fracture resistance. Previous studies found beagles treated with RAL had higher bound water in their bones [20] and ex vivo exposure of bone to RAL also increased bound water [21]. Bound water is associated with the interfaces of collagen and mineral or within the collagen triple helical structure [22]. Removing bound water through dehydration has been shown to cause an embrittlement in bones [23] as it prevents crack bridging and sliding between mineral crystals and collagen [24]. Enhancing bound water may allow for better load sharing between collagen and mineral, improving the ductility and toughness of bone.

There is a need to improve the quality and quantity of the bone given the structural and quality deficiencies of OI. Mechanical loading can be a potent anabolic stimulus in bone. There is limited data regarding mechanosensitivity in OI mice, but it may be detrimentally impacted due to alterations in the lacunar-canalicular network, impaired osteoblastogenesis, and poor collagen quality [25–31]. There has been work indicating that the lacunar-canalicular network is altered with OI, as models have shown increased lacunar density and altered lacunae shape [25]. The osteocyte is important to bone's anabolic response to mechanical stimuli and alterations to the lacunar-canalicular network in OI could alter bone's ability to sense loads [32]. Additionally, osteoblastogenesis may be impaired in OI, which would also decrease the ability to form new bone in response to loads [26]. Furthermore, altered collagen may not be able to transmit forces as effectively. These factors may be the reason that previous work with exercise has indicated that OI mice build less bone with treadmill running [27–29]. However, it is difficult to isolate the effects of

mechanical loading alone when utilizing exercise models as these models affect muscle and cardiovascular factors as well. In vivo axial tibial compression can be utilized to investigate the isolated effects of mechanical loading [33].

Given that loading can improve the quantity of bone[33, 34] and RAL may improve the quality[19, 21, 35], these approaches were combined to test the hypothesis that combination treatment would be more effective than either treatment alone. The tibiae of male and female wild-type mice and mice from the moderate G610C+/- model of OI aged 10 weeks were mechanically stimulated for six weeks. The G610C+/- is a model of moderate OI with a mutation on the alpha-2 chain of collagen that results in lower areal bone mineral density (aBMD), bone area, strength, and toughness [36–38]. A subset of these animals were simultaneously treated with RAL. We measured the structural and mechanical properties of whole bone to determine the overall effect of combination treatment of loading and RAL. To determine if loading or RAL had a greater effect on bone formed during loading or pre-existing bone, the local nanomechanical properties and chemical composition of the tissue were measured with a colocalized Raman/nanoindentation system. Finally, osteocyte lacunar geometry and apoptosis were measured to determine mechanisms of OI bone's response to loading. We predicted there would be improvements to bone quality with combination treatment, but a less robust response to loading in OI bone due to OI-induced changes in the osteocyte network and cell response.

2. Methods

2.1. Animals

2.1.1 Animal breeding and tibial loading—G610C+/- (OI) and wild-type (WT) animals were bred using female C57BL/6J mice from The Jackson Laboratory and male G610C+/- mice received from the laboratory of Dr. Alexander Robling. Female WT are used for breeding as homozygous mice from heterozygous breeding pairs die in utero [36]. Mice were group-housed with littermates of the same sex with no more than 5 mice per cage. Mice were kept on a 12-hour light/dark cycle at standard temperature and were given food and water ad libitum. A set of 4–7 mice per genotype and sex were euthanized at 10 weeks of age for a load strain calibration as previously described [39]. Briefly, a single element strain gauge was attached to the right tibia of each mouse at the cortical mid-shaft. The loads needed to engender a strain of 1390 $\mu\epsilon$ [40] were determined by measuring the strain generated by cyclic loads ranging from 1 N to 15 N. A standard curve generated for each group (Supplemental Figure 1) indicated the following forces were needed: 7.8 N for female OI mice, 10.6 N for female WT mice, 11.9 N for male OI mice, and 12.4 N for male WT mice. Mice from each group were subjected to in vivo axial tibial compressive loading of the right tibia under isoflurane-induced anesthesia for 6 weeks starting at 10 weeks of age. The left tibia served as an internal, non-loaded control. Mice were loaded three times a week with at least a day of rest between each loading day. After the first bout of loading, all mice received an intraperitoneal (IP) injection of 0.6% calcein to locate the bone's surface at the start of interventions. Four loading cycles were delivered at 4 Hz between 0.3 N and the loads indicated above, followed by 1.75 seconds of rest. This process was repeated 50 times for a total of 200 loading bouts. We have previously

found this loading protocol causes significant increases to the overall bone geometry [41]. While our later papers have indicated that changes to bone geometry are still present with only 4 weeks of loading, a 6 week duration was used here to ensure OI mice would build bone. Concurrently, mice were separated into untreated and RAL-treated groups. RAL-treated mice were given subcutaneous injections of RAL (0.5 mg/kg suspended in 10% hydroxypropyl β cyclodextrin, Sigma Aldrich) five times a week. Sample sizes were n=13 untreated OI females, n= 13 RAL-treated OI females, n=10 untreated OI males, and n=11 RAL-treated OI males. Animals were weighed weekly to determine the proper dose. Animals were euthanized at 16 weeks by cardiac exsanguination under isoflurane anesthesia followed immediately by cervical dislocation. All protocols and procedures were performed with prior approval from the Indiana University – Purdue University Indianapolis School of Science Institutional Animal Care and Use Committee (IACUC).

2.1.2 Tissue Collection—Tibiae were collected, removed of soft tissue, and stored in phosphate buffer solution (PBS)-soaked gauze at -20°C for bending tests. For female mice, tibiae from an additional set of loaded mice were cut in half at the midshaft using a low-speed sectioning saw (Buehler Isomet) immediately after dissection and soft-tissue removal. Only females were utilized given that greater differences were observed in the bending mechanics, and slow breeding of male mice made using males infeasible. The proximal half was stored in PBS-soaked gauze at -20°C for Raman spectroscopy and nanoindentation measurements and the distal half was fixed in 10% neutral buffer formalin (NBF) for 48 hours prior to being stored in 70% ethanol at room temperature for immunohistochemical assessment of osteocyte apoptosis. The uterus was extracted and weighed for female mice. Untreated female OI microcomputed tomography and mechanics of the tibiae data was previously published [42].

2.2 Microcomputed tomography (microCT)

Tibiae were scanned with a 0.5 aluminum filter, beam energy at 60 kV, beam current at 167 μA , a rotation step of 0.7° , frame averaging of 2, and with a $9.8\ \mu\text{m}$ voxel size on a Skyscan 1172 μCT system (Bruker, Billerica, MA). Hydroxyapatite phantoms at concentrations of $0.25\ \text{g}/\text{cm}^3$ and $0.75\ \text{g}/\text{cm}^3$ were scanned weekly for tissue mineralization density (TMD) calculations. Bones were reconstructed (NRecon software) and rotated (DataViewer) such that each tibia was straight and the anterior side of each was oriented in the same direction. A 1 mm trabecular region of interest (ROI) was analyzed using CTan software starting at the distal end of the growth plate. A 0.1 mm cortical ROI was analyzed at 37.5% of the length of the tibiae from the proximal end using a custom Matlab script. Trabecular parameters of bone volume fraction (BV/TV), trabecular number (Tb.N), trabecular spacing (Tb.Sp), trabecular thickness (Tb.Th), and trabecular TMD (Tb.TMD), and cortical bone structural parameters of total area, marrow area, cortical area, cortical thickness, minimum and maximum moment of inertia (I_{min} , I_{max}), bone volume fraction (BA/TA), and cortical TMD (Ct.TMD) were calculated[43].

2.3 Mechanical Testing of Tibiae

Following μCT , the same tibiae were loaded in 4 point bending until failure at a displacement rate of 0.025 mm/sec with the medial surface in tension (TA Instruments

ElectroForce 3200). Load and displacement were recorded. The upper span and lower spans were approximately 3 mm and 9 mm, respectively. Bones were hydrated with PBS during the test process. After the bones were broken, the fracture site was located relative to the proximal end of the bone using calipers, and cross-sectional data at this location measured from μ CT were used to calculate stress and strain from the load and displacement data [44]. The yield point was calculated using the 0.2% offset method based on the stress-strain curve. Bending tests were utilized so that overall mechanics along with estimated tissue-level material properties[45] could be calculated. Bending tests on bone lead to failure in tension, which is where bone is weakest and thus most likely to break clinically[46].

2.4 Colocalized Raman spectroscopy and nanoindentation

The proximal half of fresh frozen tibiae from females (n=5 untreated OI, n=5 RAL-treated OI) were embedded (without dehydration or infiltration) using a quick-setting two-part epoxy system (Koldmount). Transverse sections were then cut at 37.5% of the length of the tibiae from the proximal end using a low-speed sectioning saw (Buehler Isomet) and polished using silicon-carbide sandpaper followed by water-based diamond suspensions (3 μ m and 0.05 μ m) to a final thickness of approximately 2 mm. Samples were rinsed with deionized (DI) water between each step and sonicated in PBS for 5 minutes after polishing to remove polishing residues. Samples were refrozen in PBS-soaked gauze until measurement. Chemical composition and mechanical properties were measured using a colocalized Raman Spectroscopy (Renishaw inVia confocal Raman microscope, Wotton-under-Edge, United Kingdom) and nanoindentation system (Bruker Hysitron TI 980 TriboIndenter, Billerica, MA) as described elsewhere [47]. Using the calcein label as a marker, 8 measurements were made in new bone formed during treatment and 8 measurements were made in pre-existing bone. Samples were placed in a petri dish with the 37.5% length portion pointing up. Raman spectra were collected using a 785 nm laser (50% laser power) from 6 accumulations, each with a 10 second exposure time. Baseline correction was performed using an 11th order polynomial curve and followed by cosmic ray removal on the Renishaw WiRE software. Subsequent analysis was performed using a custom Matlab code. Smoothing was performed using a modified Savitzky-Golay function [47]. The following metrics were calculated: mineral to matrix ratio (MMR) based on phosphate (ν 1- PO_4^{3-} at 959 cm^{-1}) divided by Amide I (1665 cm^{-1}) (MMR1), CH_2 (1450 cm^{-1}) (MMR2), or Amide III (1246 cm^{-1}) (MMR3); type B carbonate substitution (ν 1- CO_3^{2-} / ν 1- PO_4^{3-} , ν 1- CO_3^{2-} at 1071 cm^{-1}); and crystallinity (inverse of the full width half max (FWHM) of ν 1- PO_4^{3-} band) as previously described [41]. Ratios were calculated using peak areas.

After Raman collection, samples were hydrated with PBS and nanoindentation was performed using a spherical diamond probe with a 1.03 μ m radius. Samples were loaded to a force of 1000 μ N at a rate of 200 μ N/sec, held at 1000 μ N for 30 seconds, and released at a rate of 200 μ N/sec. Load and displacement were recorded and elastic modulus (Er) and hardness were calculated based on Oliver-Pharr method [48]. Dissipated energy was calculated by obtaining the hysteresis area between the loading and unloading curves [49] using customized Matlab code.

2.5 Osteocyte apoptosis

Bones were stained for annexin V, which has been previously utilized as a measure of osteocyte apoptosis [50, 51]. The fixed distal half of the tibiae samples were demineralized in 14% EDTA for two weeks at 4°C. Samples were embedded in paraffin and sectioned in transverse cross-sections from the proximal end (approximate midshaft) at a thickness of approximately 5 µm. Samples were immunostained using the avidin-biotin method and incubated with rabbit polyclonal anti-annexin V (Abcam, Cambridge, MA, USA) as previously described [52]. Counterstaining was done with methyl green and the percentage of osteocytes labeled with annexin V out of the total number of osteocytes within the cross-section was reported.

2.6 Quantitative backscatter electron imaging (qBEI)

After nanoindentation, the embedded tibiae samples were rinsed to remove excess salt from PBS and dehydrated under a vacuum for 48 hours. These sections were then imaged with qBEI using a BED-C retractable backscatter electron detector on a scanning electron microscope (SEM) (JEOL 7800F, Tokyo, Japan). Current voltage was 10 kV and probe current was 13 µA. Images were taken at a magnification of 200X on the posterior lateral side of the cross-section, where peak strains are likely to occur [33]. Aluminum and carbon standards were imaged using the same settings. Contrast and brightness were held constant for all samples during imaging. After scanning, contrast was adjusted so that carbon had average intensity values of 25 ± 1 and aluminum had intensity values of 225 ± 1 using a custom Matlab script. The same contrast adjustment was applied to all sample images. Intensity values were converted to percent calcium (%Ca) values based on the atomic numbers for carbon ($Z=6$) and aluminum ($Z=13$) being set at known intensity values as described by others [53]. Images were then analyzed in a user-chosen ROI for bone mineral density distribution (BMDD) measurements of Ca_{mean} (weighted average), Ca_{peak} (most common Ca value), and FWHM of the intensity curve to measure mineral heterogeneity. After the BMDD values were calculated, the program calculated measurements on the lacunar network. Briefly, the image was binarized, and upper and lower size limits were set to eliminate shapes either too large or too small to be lacunae. User input was used to eliminate any objects deemed to be artifacts and Matlab analysis was used to analyze object properties. Lacunar measurements of lacunar number, lacunar density (number divided by ROI), average lacunar area, lacunar area percent (total area of lacunae divided by ROI times 100), average lacunar perimeter, and circularity were calculated.

2.7 Statistics

Unpaired Students' t tests were used to determine differences in body weight and uterus weight for untreated and RAL-treated OI animals. Repeated measures two-way ANOVAs were used to analyze the main effects of loading, RAL treatment, and interaction effects within each genotype. Loaded and non-loaded measures on the same animal were the repeated measure. RAL comparisons were made between mice. All statistics were performed using GraphPad Prism software. Average and standard deviations of OI data are represented in the tables and graphs. Dashed lines represent average and standard deviations of WT animals on graphed data. WT animals were loaded and treated with RAL and all data

are available in the supplemental materials; however, WT data are not reported in the main results section given the complexity of the study, the number of comparisons being made, and our focus on how combination treatment affects OI mice. Cohen's D effect sizes were calculated by dividing the differences between the means by the pooled standard deviation. Effect sizes below 1 were considered mild, while those larger than 1 were highlighted to emphasize compelling differences. Repeated measures three-way ANOVAs were used to analyze Raman/nanoindentation data, with main effects of loading, RAL, and age of bone and interaction effects being determined. These comparisons were done within each genotype. Repeated measures were loaded and non-loaded limbs while age of bone and RAL treatment were considered non-repeated measures.

3. Results

3.1 Body weight decreased and uterus weight percent increased with RAL treatment in OI female mice

Final body weight was 20.4 ± 1.1 g for female untreated OI mice and 19.4 ± 1.1 g for female RAL-treated OI mice. The uterus weight was 76.1 ± 22.4 mg for untreated female OI mice and 92.5 ± 27.7 mg for female RAL-treated OI mice. The uterus body weight percent was $0.377 \pm 0.112\%$ for untreated OI mice and $0.475 \pm 0.145\%$ for RAL-treated OI mice. Final body weight ($p=0.021$) and uterus body weight percent ($p=0.036$) were significantly different between RAL and untreated groups in female mice. For males, untreated OI mice had a final body weight of 24.9 ± 1.2 g and RAL-treated OI mice had a final body weight of 25.3 ± 1.7 g (difference not significant). Comparatively, RAL-treatment was not a significant factor for WT mice for body weight, uterus weight, or uterus weight percent though these trended lower for RAL-treated mice (Supplemental Table 1).

3.2 Loading improved cortical bone structural properties and both loading and RAL-treatment improved trabecular bone structural properties

Cortical area was higher with loading in both untreated and RAL-treated OI female and male mice (Figure 1A, Figure 1B). Loading was the main factor affecting cortical bone structure as total area in both sexes, marrow area in females, and I_{\min} and I_{\max} in both sexes were all altered with loading (Figure 1, Table 1). Data from microCT and mechanical tests for OI mice that had no significant differences are reported in Supplemental Table 2. Similarly, loading was the main factor affecting cortical bone in WT mice (Supplemental Table 3). Ct.TMD was the only cortical bone property altered with RAL treatment (Figure 1E) in OI mice, and was higher in RAL-treated females but did not change in males (Figure 1E, Figure 1F). In WT mice, Ct. TMD was not altered with loading or RAL treatment. RAL treatment only increased cortical thickness in male WT non-loaded tibiae (Supplemental Table 3).

Loading and RAL-treatment were significant factors for multiple properties in trabecular bone. Loading and RAL-treatment both increased BV/TV in male and female OI mice (Table 1). In females, loading increased trabecular thickness whereas RAL increased trabecular number (Table 1). In males, loading increased trabecular number and decreased spacing, whereas RAL treatment only increased trabecular number (Table 1). Loading increased BV/TV and trabecular thickness and decreased trabecular spacing in male and

female WT mice. RAL-treatment increased trabecular thickness in male and female WT mice and BV/TV in female mice (Supplemental Table 3). Effect sizes were generally higher in OI males with loading and RAL-treatment compared to loading or RAL-treatment alone for both cortical and trabecular properties (Table 2). In females, it varied whether loading or loading combined with RAL-treatment had the greatest effect (Table 2). The largest effect in female was observed in trabecular BV/TV with both loading and RAL-treatment (Table 2). Like in OI mice, loading and RAL-treatment in WT mice had the largest effect compared to loading or RAL-treatment alone (Supplemental Table 4). Percent change and effect sizes were larger in WT mice compared to OI mice (Table 2, Supplemental Table 4).

3.3 Loading only increased ultimate force in female mice whereas RAL improved yield stress and resilience in females.

Whole bone mechanical properties were largely unaffected by loading or RAL treatment in either sex. Ultimate force was higher in loaded females but not impacted in males with loading or treatment (Figure 2). Yield displacement was decreased with RAL-treatment in non-loaded male tibiae and decreased with loading in untreated males (Table 3). No other whole bone properties were impacted with loading or treatment in either sex (Supplemental Table 2). This observation was similar to WT results where loading was a significant factor for females but not males (Supplemental Table 5). Interestingly, RAL-treatment was a significant factor for ultimate force in WT males. In females, RAL improved yield stress and resilience (Table 3). Ultimate stress trended higher in female mice with RAL treatment (Figure 2C, $p=0.06$). For males, the only change in material properties was that resilience was lower in loaded untreated OI mice compared to non-loaded untreated mice (Table 3). RAL-treatment was not a significant factor for WT mice (Supplemental Table 6). Most effect sizes were greater with loading and RAL-treatment compared to loading alone in females but impacts in males were variable (Table 2).

3.4 Localized nanoindentation measurements did not show improvements with RAL treatment in either new or old bone

There were few differences in MMR values with loading or RAL-treatment as seen in Figure 3 and Supplemental Table 7. However, $\nu 1\text{PO}_4^{3-}/\text{CH}_2$ was lower in new bone with loading in RAL-treated animals (Figure 3D). Loading was a significant factor with Er (Figure 3C). For most groups, loading lowered Er with the exception of new bone areas in untreated mice (Figure 3C). Bone age was not an independent significant factor but contributed to interaction effects for OI mice. Hardness was lower with loading in old bone in untreated OI mice and dissipated energy was greater with loading in old bone in untreated OI mice (Figure 3). Interestingly, there were fewer changes in WT mice as seen in Supplemental Table 8. Loading increased hardness in WT mice and decreased dissipated energy.

3.5 Osteocyte apoptosis was altered with both loading and RAL-treatment, but lacunar geometry was not changed

RAL-treatment decreased osteocyte apoptosis in non-loaded female mice, an effect not seen in the loaded limbs (Figure 4). Loading increased apoptosis in RAL-treated mice but did not impact apoptosis in untreated females (although apoptosis trended up). An important observation is that the average WT apoptosis measurements were lower than all

OI groups (Figure 4). WT mice showed similar increases in annexin V staining with loading (Supplemental Figure 2), but RAL-treatment increased apoptosis in WT mice. qBEI did not indicate any differences in lacunar geometry or mineralization with either loading or RAL-treatment in OI mice (Supplemental Figure 3, Supplemental Table 9). Increases in lacunar number with loading in OI mice are likely the result of increased bone size (Supplemental Table 9). Only Ca_{mean} increased with loading in WT untreated mice (Supplemental Table 10).

4. Discussion

Combination treatment with loading and RAL improved bone structural properties as measured by μ CT and importantly, some material properties in female OI mice. There were positive structural changes observed in both males and females in bone geometry where effect sizes indicate that loading and RAL-treatment combined had a greater effect than either loading or RAL-treatment alone. Cortical structure was improved with loading in both males and females. Effect sizes for properties including cortical thickness, bone area, and I_{max} were higher in males with loading and RAL-treatment than in females with loading and RAL-treatment. This observation is consistent with previous work from the laboratory, which indicated that RAL and loading both increased the amount of cortical bone in C57BL/6J male mice, but loading drove the changes in female cortical bone [41]. However, unlike the previous study, the current study did not reach statistical significance for RAL-treatment in WT males for cortical bone structure (Supplemental Table 3), despite increasing trends. Effect sizes compared to WT mice (Table 2, Supplemental Table 4) indicate that OI mice had a less robust response to loading than WT. This is consistent with a previous study finding that OI mice had diminished muscle building and did not improve bone structure with exercise [29]. Another study similarly showed that exercise had no effect on femoral bone structure of OI mice [28]. This less robust response to anabolic stimuli in bone is likely due to the underlying cellular changes and bone quality defects observed in OI.

Increases in trabecular bone volume were greater when combining RAL-treatment and loading versus loading or RAL-treatment alone in both males and female OI mice. The greater effect observed with RAL-treatment and loading on trabecular bone compared to cortical bone could be due to the increased surface area available in trabecular bone. Previous in vitro work has indicated that RAL increases osteoblast proliferation and decreases osteoclast proliferation [54]. A greater surface area in trabecular bone gives more area for osteoblast activity to occur. The improvement of trabecular bone with RAL-treatment is consistent with clinical results indicating BMD improvements with RAL-treatment [55]. In females, loading increased BV/TV by changing trabecular thickness whereas RAL increased trabecular number (Table 1). In males, RAL and loading both increased BV/TV and trabecular number. Unlike cortical bone, loading increased TMD in trabecular bone.

Loading increased the ultimate force in both untreated and RAL-treated females but not in males. This extrinsic mechanical property is driven primarily by the quantity and geometry of the bone, in addition to tissue quality measures such as mineralization. Female OI mice

were able to build bone in response to loading, though this response was less robust than female WT mice as seen by the differences in effect sizes (Table 2, Supplemental Table 4). While males were also able to build bone in response to loading (Figure 1, Table 1), this did not translate to an increase in ultimate force. As with females, male OI mice had a less robust response to loading when compared to WT males (Table 2, Supplemental Table 4). The lack of an increase in ultimate force could be because male OI mice already had a fairly high I_{\min} (Figure 1D) and therefore the percent change was lower with a smaller effect size observed with loading (Table 2). Moment of inertia reflects the distribution of bone material away from the centroid of the bone. The larger the value, the lower the stress for a given load which is beneficial to fracture resistance [45].

Intrinsic material properties of whole bone were not altered with loading in either male or female mice. This lack of change is not surprising, as loading tends to add more bone, but does not necessarily improve tissue quality. RAL did improve some material properties in female OI mice. Specifically, resilience and yield stress increased with RAL treatment, and ultimate stress trended up (Table 3, Figure 2). This increase in yield stress and resilience could be due to the increase in Ct.TMD observed with raloxifene treatment, as mineralization strongly contributes to strength [56], and previous work has shown that higher mineralization results in greater strength [57]. Neither loading nor raloxifene improved properties typically associated with collagen (e.g. total strain or toughness; Supplemental Table 2, Figure 2). This lack of impact on collagen is unfortunate given that this model of OI has defects in post-yield properties and displays brittle behavior [38]. However, it should be noted that when comparing to untreated, non-loaded mice, combination treatment exhibited greater increases in effect size in female mice compared to loading alone (Table 2). It should also be noted that the increases in Ct.TMD with RAL did not result in a loss of toughness which can occur with greater mineralization, indicating that RAL may have preserved toughness while increasing strength.

It is possible that RAL treatment only improved the quality of newly formed bone and not bone formed prior to treatment. To test this, colocalized Raman/nanoindentation was used to assess the chemical and nanomechanical properties in old bone and new bone in OI mice. Given that more mechanical changes were observed in female OI mice and breeding in male OI mice was extremely slow, these properties were only assessed in female mice. There were few changes to the chemical composition of mineral. Loading and bone age had a positive interaction effect on crystallinity, but individual posthoc comparisons indicated no differences (Supplemental Table 7). Loading decreased MMR2 ($\nu_1\text{PO}_4^{3-}/\text{CH}_2$) in OI RAL-treated new bone compared to non-loaded OI RAL-treated new bone (Figure 3). Interestingly, nanomechanical properties were different with loading but were not impacted with RAL treatment in new or old bone. As seen in Figure 3, loading was a significant factor for Er. For most groups, loading decreased elastic modulus but since there was no significant interaction, individual comparisons were not made. The lower modulus would normally reflect a decrease in MMR which was not observed. However, other factors such as mineral quality that are not captured by MMR may have contributed. This is in contrast to the WT mice, where there were no differences observed in Raman properties, but loading affected hardness and dissipated energy, which were higher and lower with loading, respectively (Supplemental Table 8). Modulus trended higher for loading, but was

significantly different for the age of bone, where old bone had higher modulus than new bone. For nanoindentation, modulus is related to the level of mineral which would indicate the older bone had more time to mineralize. Hypermineralization in OI often results in brittle behavior, so a decrease in modulus observed in OI mice could be an indicator that mineral quality was beginning to improve. However, newly formed loaded bone had higher modulus than new non-loaded bone in untreated OI mice. This would indicate the changes in loading were site specific or that RAL prevented increases in modulus in new bone formed during loading bone.

To explore why the response to loading was less robust in OI mice, we assessed osteocyte apoptosis using annexin V staining. Osteocyte apoptosis is altered with mechanical loading and unloading and is required for bone remodeling in response to microdamage [58–60]. Osteocyte apoptosis is believed to follow a U-shaped curve in which unloading causes increases in apoptosis and loads at high enough levels to cause microdamage increase apoptosis as well[58]. Poor bone quality may make the response to loading less robust since low-quality bone may not efficiently transmit forces to the osteocyte. Results indicate that OI mice have naturally higher levels of osteocyte apoptosis (Figure 4), which may have contributed to their less robust response to mechanical stimuli. Loading did not significantly increase osteocyte apoptosis in untreated animals. However, RAL-treatment appeared to lower non-loaded levels of osteocyte apoptosis to values similar to that of WT non-loaded bones (Figure 4). Thus, RAL-treated animals demonstrated an increase in apoptosis with loading. Our results differ from a previous study in which the ulnae of rats were loaded to approximately 3000 $\mu\epsilon$ and osteocyte apoptosis decreased[61]. However, they are in agreement with other studies that found osteocyte apoptosis increased with fatigue loading that caused microdamage at approximately 3300–3800 $\mu\epsilon$ [59, 60]. This could indicate that our loading regimen produced microdamage. The changes seen in osteocyte apoptosis could contribute to the larger effect sizes observed with RAL and loading in female OI mice for cortical structure (Table 2). Previous research has indicated that RAL may decrease apoptosis [62]. This is an interesting effect that should be investigated further. The differences observed in osteocyte apoptosis did not appear to be the result of lacunar geometry, as there were few changes observed with loading or RAL-treatment in OI mice (Supplemental Table 9, Supplemental Figure 3). Lacunar geometry affects the stresses transmitted to the osteocyte and may have been a factor in the differences in apoptosis and loading response [63–65]. The differing levels of apoptosis could be a contributing factor to the less robust response in changes to bone structure observed in OI mice compared to WT mice, as seen through differences in effect sizes.

Limitations of this study include the loss in signal observed with colocalized Raman/nanoindentation measurement. This increased the variability of measurements and prevented accurate reporting of Raman measurements based on subpeak ratios. Additionally, we were not able to directly assess whether woven bone formation occurred, which is an aspect of bone quality that might not be easily captured with microCT. The storage conditions required for mechanics and the slow breeding of the animals prevented the collection of more samples or samples stored in conditions that would allow for more histological assessments. However, this study gives an initial point to examine the effects of in vivo tibial loading and RAL-treatment on OI mice that future studies can build upon.

5. Conclusions

Overall, combination treatment with RAL and mechanical loading produced subtle improvements to bone quality in OI mice as observed through higher effect sizes seen with RAL and loading compared to untreated non-loaded mice. More changes occurred in female versus male mice, which could have been either due to the differing effects of SERM treatment between sexes or due to sex differences in bone structure. While nanoindentation did not indicate any differences with RAL treatment in old versus new bone, loading resulted in decreased elastic modulus in both tissue types. OI mice likely exhibited a less robust response to loading due to naturally high osteocyte apoptosis that was decreased with RAL treatment. Overall, combination therapy should be considered in the future of therapeutics for OI.

Supplementary Material

Refer to Web version on PubMed Central for supplementary material.

Acknowledgments

This work was supported by the National Institute of Health (NIH) [JMW:AR072609]. AC was supported by NIH T32 AR065971. The authors would like to thank the Integrated Nanosystems Development Institute (INDI) for the use of their scanning electron microscope, which was awarded through NSF grant MRI-1229514.

7. References

1. Forlino A and Marini JC, Osteogenesis imperfecta. *The Lancet*, 2016. 387(10028): p. 1657–1671.
2. Bishop N, Bone Material Properties in Osteogenesis Imperfecta. *Journal of Bone and Mineral Research*, 2016. 31(4): p. 699–708. [PubMed: 26987995]
3. Fratzl-Zelman N, Schmidt I, Roschger P, Glorieux FH, Klaushofer K, Fratzl P et al. , Mineral particle size in children with osteogenesis imperfecta type I is not increased independently of specific collagen mutations. *Bone*, 2014. 60: p. 122–128.
4. Imbert L, Auregan J-C, Pernelle K, Hoc T, Mechanical and mineral properties of osteogenesis imperfecta human bones at the tissue level. *Bone*, 2014. 65: p. 18–24. [PubMed: 24803077]
5. Blouin S, et al. , Hypermineralization and High Osteocyte Lacunar Density in Osteogenesis Imperfecta Type V Bone Indicate Exuberant Primary Bone Formation. *Journal of Bone and Mineral Research*, 2017. 32(9): p. 1884–1892. [PubMed: 28548288]
6. Morello R, Osteogenesis imperfecta and therapeutics. *Matrix Biology*, 2018. 71–72: p. 294–312.
7. Roschger A, et al. , Effect of sclerostin antibody treatment in a mouse model of severe osteogenesis imperfecta. *Bone*, 2014. 66: p. 182–188. [PubMed: 24953712]
8. Jacobsen CM, et al. , Targeting the LRP5 pathway improves bone properties in a mouse model of osteogenesis imperfecta. *Journal of bone and mineral research : the official journal of the American Society for Bone and Mineral Research*, 2014. 29(10): p. 2297–2306. [PubMed: 24677211]
9. Kaupp S, et al. , Combination therapy in the Col1a2G610C mouse model of Osteogenesis Imperfecta reveals an additive effect of enhancing LRP5 signaling and inhibiting TGF β signaling on trabecular bone but not on cortical bone. *Bone*, 2020. 131: p. 115084. [PubMed: 31648079]
10. Tauer JT, Abdullah S, and Rauch F, Effect of Anti-TGF- β Treatment in a Mouse Model of Severe Osteogenesis Imperfecta. *Journal of Bone and Mineral Research*, 2019. 34(2): p. 207–214. [PubMed: 30357929]
11. Greene B, et al. , Inhibition of TGF- β Increases Bone Volume and Strength in a Mouse Model of Osteogenesis Imperfecta. *JBMR Plus*, 2021. 5(9): p. e10530. [PubMed: 34532615]

12. Glorieux FH, et al. , BPS804 Anti-Sclerostin Antibody in Adults With Moderate Osteogenesis Imperfecta: Results of a Randomized Phase 2a Trial. *Journal of Bone and Mineral Research*, 2017. 32(7): p. 1496–1504. [PubMed: 28370407]
13. Seeman E, Raloxifene. *Journal of Bone and Mineral Metabolism*, 2001. 19(2): p. 65–75. [PubMed: 11281162]
14. Liu JH, Selective estrogen receptor modulators (SERMS): keys to understanding their function. *Menopause*, 2020. 27(10).
15. Khosla S, Oursler MJ, and Monroe DG, Estrogen and the skeleton. *Trends in Endocrinology & Metabolism*, 2012. 23(11): p. 576–581. [PubMed: 22595550]
16. Gallant MA, Brown Drew M., Hammond Max, Wallace Joseph M., Du Jiang, Deymier-Black Alix C., Almer Jonathan D., Stock Stuart R., Allen Matthew R., Burr David B., Bone cell-independent benefits of raloxifene on the skeleton: A novel mechanism for improving bone material properties. *Bone*, 2014. 61: p. 191–200. [PubMed: 24468719]
17. Hill Gallant KM, Gallant Maxime A., Brown Drew M., Sato Amy Y., Williams Justin N., Burr David B., Raloxifene Prevents Skeletal Fragility in Adult Female Zucker Diabetic Sprague-Dawley Rats. *PLOSOne*, 2014. 9(9).
18. Meixner CN, et al. , Raloxifene Improves Bone Mechanical Properties in Mice Previously Treated with Zoledronate. *Calcified tissue international*, 2017. 101(1): p. 75–81. [PubMed: 28246928]
19. Berman AG, et al. , Raloxifene reduces skeletal fractures in an animal model of osteogenesis imperfecta. *Matrix Biology*, 2016. 52–54: p. 19–28.
20. Allen MR, et al. , In Vivo UTE-MRI Reveals Positive Effects of Raloxifene on Skeletal-Bound Water in Skeletally Mature Beagle Dogs. *Journal of Bone and Mineral Research*, 2015. 30(8): p. 1441–1444. [PubMed: 25644867]
21. Surowiec RK, et al. , Ex vivo exposure to calcitonin or raloxifene improves mechanical properties of diseased bone through non-cell mediated mechanisms. *Bone*, 2023. 173: p. 116805. [PubMed: 37196853]
22. Surowiec RK, Allen MR, and Wallace JM, Bone hydration: How we can evaluate it, what can it tell us, and is it an effective therapeutic target? *Bone Rep*, 2022. 16: p. 101161. [PubMed: 35005101]
23. Nyman JS, et al. , Partial removal of pore and loosely bound water by low-energy drying decreases cortical bone toughness in young and old donors. *Journal of the Mechanical Behavior of Biomedical Materials*, 2013. 22: p. 136–145. [PubMed: 23631897]
24. Maghsoudi-Ganjeh M, Wang X, and Zeng X, Computational investigation of the effect of water on the nanomechanical behavior of bone. *Journal of the Mechanical Behavior of Biomedical Materials*, 2020. 101: p. 103454. [PubMed: 31586882]
25. Carriero A, et al. , Altered lacunar and vascular porosity in osteogenesis imperfecta mouse bone as revealed by synchrotron tomography contributes to bone fragility. *Bone*, 2014. 61: p. 116–124. [PubMed: 24373921]
26. Gioia R, et al. , Impaired Osteoblastogenesis in a Murine Model of Dominant Osteogenesis Imperfecta: A New Target for Osteogenesis Imperfecta Pharmacological Therapy. *STEM CELLS*, 2012. 30(7): p. 1465–1476. [PubMed: 22511244]
27. Jeong Y, et al. , Hindlimb Skeletal Muscle Function and Skeletal Quality and Strength in +/G610C Mice With and Without Weight-Bearing Exercise. *Journal of Bone and Mineral Research*, 2015. 30(10): p. 1874–1886. [PubMed: 25829218]
28. Tauer JT, et al. , Muscle-bone properties after prolonged voluntary wheel running in a mouse model of dominant severe osteogenesis imperfecta. *J Musculoskelet Neuronal Interact*, 2021. 21(4): p. 517–527. [PubMed: 34854391]
29. Gremminger VL, et al. , Compromised Exercise Capacity and Mitochondrial Dysfunction in the Osteogenesis Imperfecta Murine (oim) Mouse Model. *Journal of Bone and Mineral Research*, 2019. 34(9): p. 1646–1659. [PubMed: 30908713]
30. Imbert L, et al. , Microstructure and compressive mechanical properties of cortical bone in children with osteogenesis imperfecta treated with bisphosphonates compared with healthy children. *Journal of the Mechanical Behavior of Biomedical Materials*, 2015. 46: p. 261–270. [PubMed: 25828157]

31. Viguet-Carrin S, Garnero P, and Delmas PD, The role of collagen in bone strength. *Osteoporosis International*, 2006. 17(3): p. 319–336. [PubMed: 16341622]
32. Robling AG and Bonewald LF, The Osteocyte: New Insights. *Annual Review of Physiology*, 2020. 82(1): p. 485–506.
33. Main RP, et al. , Murine Axial Compression Tibial Loading Model to Study Bone Mechanobiology: Implementing the Model and Reporting Results. *Journal of Orthopaedic Research*, 2020. 38(2): p. 233–252. [PubMed: 31508836]
34. Yang H, et al. . Adaptive changes in micromechanical environments of cancellous and cortical bone in response to in vivo loading and disuse. *Journal of Biomechanics*, 2019. 89: p. 85–94. [PubMed: 31047696]
35. Tastad CA, Kohler R, and Wallace JM, Limited impacts of thermoneutral housing on bone morphology and mechanical properties in growing female mice exposed to external loading and raloxifene treatment. *Bone*, 2021. 146: p. 115889. [PubMed: 33618075]
36. Daley E, et al. , Variable bone fragility associated with an Amish COL1A2 variant and a knock-in mouse model. *Journal of Bone and Mineral Research*, 2010. 25(2): p. 247–261. [PubMed: 19594296]
37. Masci M, et al. , Bone mineral properties in growing Col1a2(+/-G610C) mice, an animal model of osteogenesis imperfecta. *Bone*, 2016. 87: p. 120–129. [PubMed: 27083399]
38. Kohler R, et al. , Morphological and mechanical characterization of bone phenotypes in the Amish G610C murine model of osteogenesis imperfecta. *PLOS ONE*, 2021. 16(8): p. e0255315. [PubMed: 34449800]
39. Berman AG, et al. , Structural and Mechanical Improvements to Bone Are Strain Dependent with Axial Compression of the Tibia in Female C57BL/6 Mice. *PloS one*, 2015. 10(6): p. e0130504–e0130504. [PubMed: 26114891]
40. Fan Y, et al. , Skeletal loading regulates breast cancer-associated osteolysis in a loading intensity-dependent fashion. *Bone Research*, 2020. 8(1): p. 9. [PubMed: 32128277]
41. Berman AG, et al. , Effects of Raloxifene and tibial loading on bone mass and mechanics in male and female mice. *Connective Tissue Research*, 2022. 63(1): p. 3–15. [PubMed: 33427519]
42. Kohler R, Creecy A, Willians DR, Allen MR, Wallace JM, Effects of Novel Raloxifene Analogs Alone or in Combination with Mechanical Loading in the Col1a2G610c/+ Murine Model of Osteogenesis Imperfecta. *Bone*, 2023.
43. Bouxsein ML, Boyd Stephen K, Christiansen Blaine A, Guldberg Robert E, Jepsen Karl J, Muller Ralph, Guidelines for assessment of bone microstructure in rodents using micro-computed tomography. *Journal of Bone and Mineral Research*, 2010. 25(7): p. 1468–1486. [PubMed: 20533309]
44. Wallace JM, et al. , Inbred Strain-Specific Response to Biglycan Deficiency in the Cortical Bone of C57BL6/129 and C3H/He Mice. *Journal of Bone and Mineral Research*, 2009. 24(6): p. 1002–1012. [PubMed: 19113913]
45. Turner CH, Burr DB, Basic Biomechanical Measurements of Bone: A Tutorial. *Bone*, 1993. 14: p. 595–608. [PubMed: 8274302]
46. Turner CH, Bone strength: current concepts. *Annals of the New York Academy of Sciences*, 2006. 1068(1): p. 429–446. [PubMed: 16831941]
47. Damrath JG, Moe SM, and Wallace JM, Calcimimetics Alter Periosteal and Perilacunar Bone Matrix Composition and Material Properties in Early Chronic Kidney Disease. *Journal of Bone and Mineral Research*, 2022. 37(7): p. 1297–1306. [PubMed: 35593150]
48. Oliver WC and Pharr GM, An improved technique for determining hardness and elastic modulus using load and displacement sensing indentation experiments. *Journal of Materials Research*, 1992. 7(6): p. 1564–1583.
49. Jha KK, et al. , Energy-based analysis of nanoindentation curves for cementitious materials. *ACI Materials Journal*, 2012. 109(1): p. 81.
50. Stanislaus D, et al. , In vivo regulation of apoptosis in metaphyseal trabecular bone of young rats by synthetic human parathyroid hormone (1–34) fragment. *Bone*, 2000. 27(2): p. 209–218. [PubMed: 10913913]

51. Metzger CE, et al. , DSS-induced colitis produces inflammation-induced bone loss while irisin treatment mitigates the inflammatory state in both gut and bone. *Scientific Reports*, 2019. 9(1): p. 15144. [PubMed: 31641205]
52. Metzger CE, Swallow EA, and Allen MR, Elevations in Cortical Porosity Occur Prior to Significant Rise in Serum Parathyroid Hormone in Young Female Mice with Adenine-Induced CKD. *Calcified Tissue International*, 2020. 106(4): p. 392–400. [PubMed: 31832725]
53. Roschger P, et al. , Validation of quantitative backscattered electron imaging for the measurement of mineral density distribution in human bone biopsies. *Bone*, 1998. 23(4): p. 319–326. [PubMed: 9763143]
54. Taranta A, et al. , The selective estrogen receptor modulator raloxifene regulates osteoclast and osteoblast activity in vitro. *Bone*, 2002. 30(2): p. 368–376. [PubMed: 11856644]
55. Sarkar S, et al. , Relationships Between Bone Mineral Density and Incident Vertebral Fracture Risk with Raloxifene Therapy. *Journal of Bone and Mineral Research*, 2002. 17(1): p. 1–10. [PubMed: 11771654]
56. Unal M, Creecy A, Nyman JS, The Role of Matrix Composition in the Mechanical Behavior of Bone. *Current Osteoporosis Reports*, 2018. 16(3): p. 205–215. [PubMed: 29611037]
57. Currey J, Effects of differences in mineralization on the mechanical properties of bone. *Philosophical Transactions of the Royal Society B*, 1984. 304(1121): p. 509–518.
58. Jilka RL, Noble B, and Weinstein RS, Osteocyte apoptosis. *Bone*, 2013. 54(2): p. 264–271. [PubMed: 23238124]
59. Kennedy OD, et al. , Activation of resorption in fatigue-loaded bone involves both apoptosis and active pro-osteoclastogenic signaling by distinct osteocyte populations. *Bone*, 2012. 50(5): p. 1115–1122. [PubMed: 22342796]
60. Kennedy OD, et al. , Osteocyte apoptosis is required for production of osteoclastogenic signals following bone fatigue in vivo. *Bone*, 2014. 64: p. 132–137. [PubMed: 24709687]
61. Noble BS, et al., Mechanical loading: biphasic osteocyte survival and targeting of osteoclasts for bone destruction in rat cortical bone. 2003. 284(4): p. C934–C943.
62. Sun Q, et al. , Raloxifene retards the progression of adjacent segmental intervertebral disc degeneration by inhibiting apoptosis of nucleus pulposus in ovariectomized rats. *Journal of Orthopaedic Surgery and Research*, 2021. 16(1): p. 368. [PubMed: 34107971]
63. Joukar A, Niroomand-Oscuii H, and Ghalichi F, Numerical simulation of osteocyte cell in response to directional mechanical loadings and mechanotransduction analysis: Considering lacunar-canalicular interstitial fluid flow. *Comput Methods Programs Biomed*, 2016. 133: p. 133–141. [PubMed: 27393805]
64. Kola SK, et al. , Osteocyte lacunar strain determination using multiscale finite element analysis. *Bone Rep*, 2020. 12: p. 100277. [PubMed: 32478144]
65. Bacabac RG, et al. , Round versus flat: Bone cell morphology, elasticity, and mechanosensing. *Journal of Biomechanics*, 2008. 41(7): p. 1590–1598. [PubMed: 18402963]

Highlights

- In vivo axial compressive loading of the tibia combined with raloxifene treatment improves bone quantity and quality in female OI mice
- Improvements were mostly with the strength of the bone, not the post-yield properties
- Osteocyte apoptosis was higher with loading in female untreated OI mice, but not in raloxifene-treated OI mice

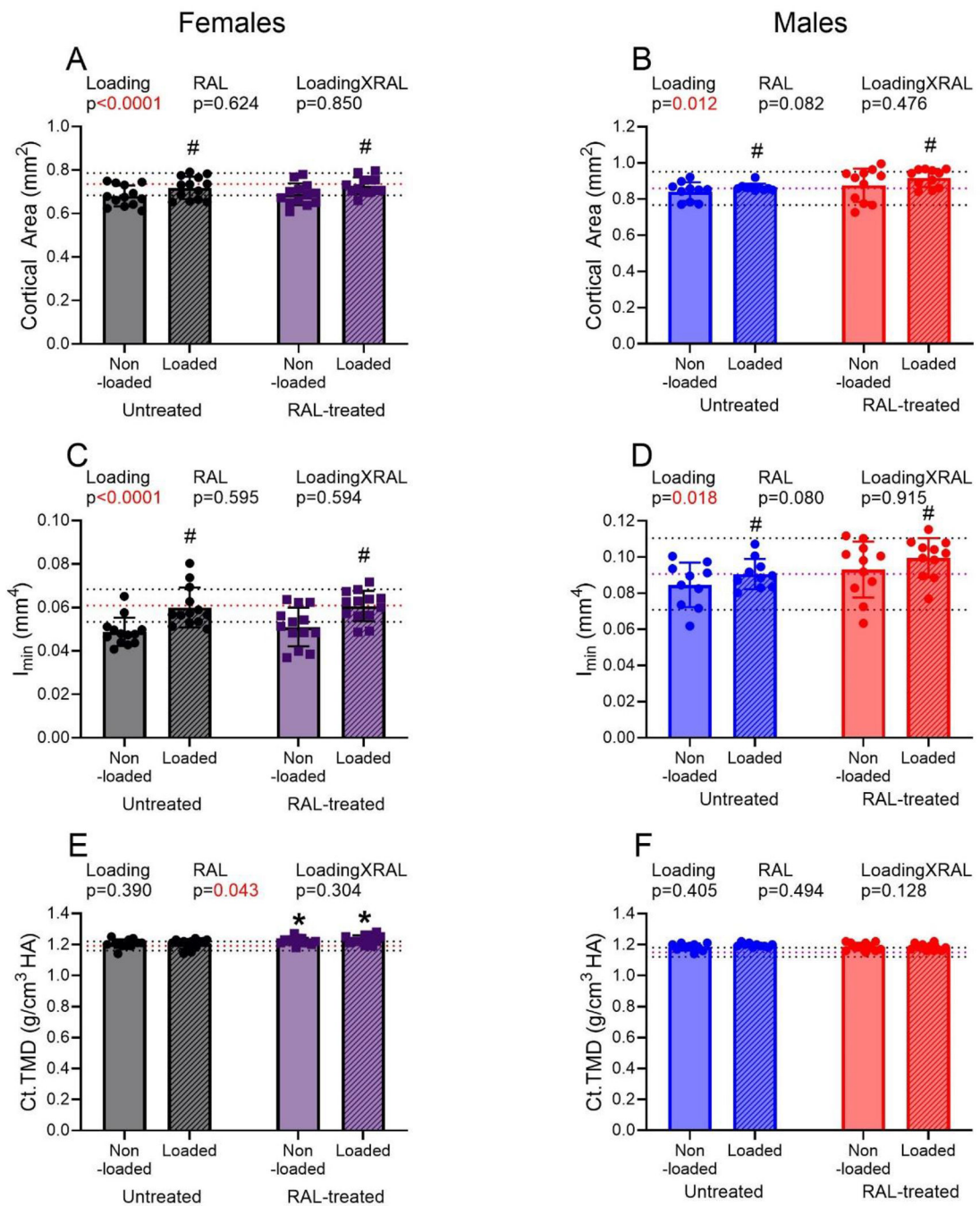


Figure 1: Cortical area (A,B), minimum moment of inertia (I_{\min}) (C,D) of cortical tissue mineralization density (Ct.TMD) (E,F) of non-loaded and loaded tibiae of male and female OI mice. # indicates difference with loading and * indicates difference with raloxifene treatment. Dotted lines on graphs indicate the average (purple/red) and standard deviations (black) of wild-type non-loaded untreated mice. Two way ANOVA p values are written over graph.

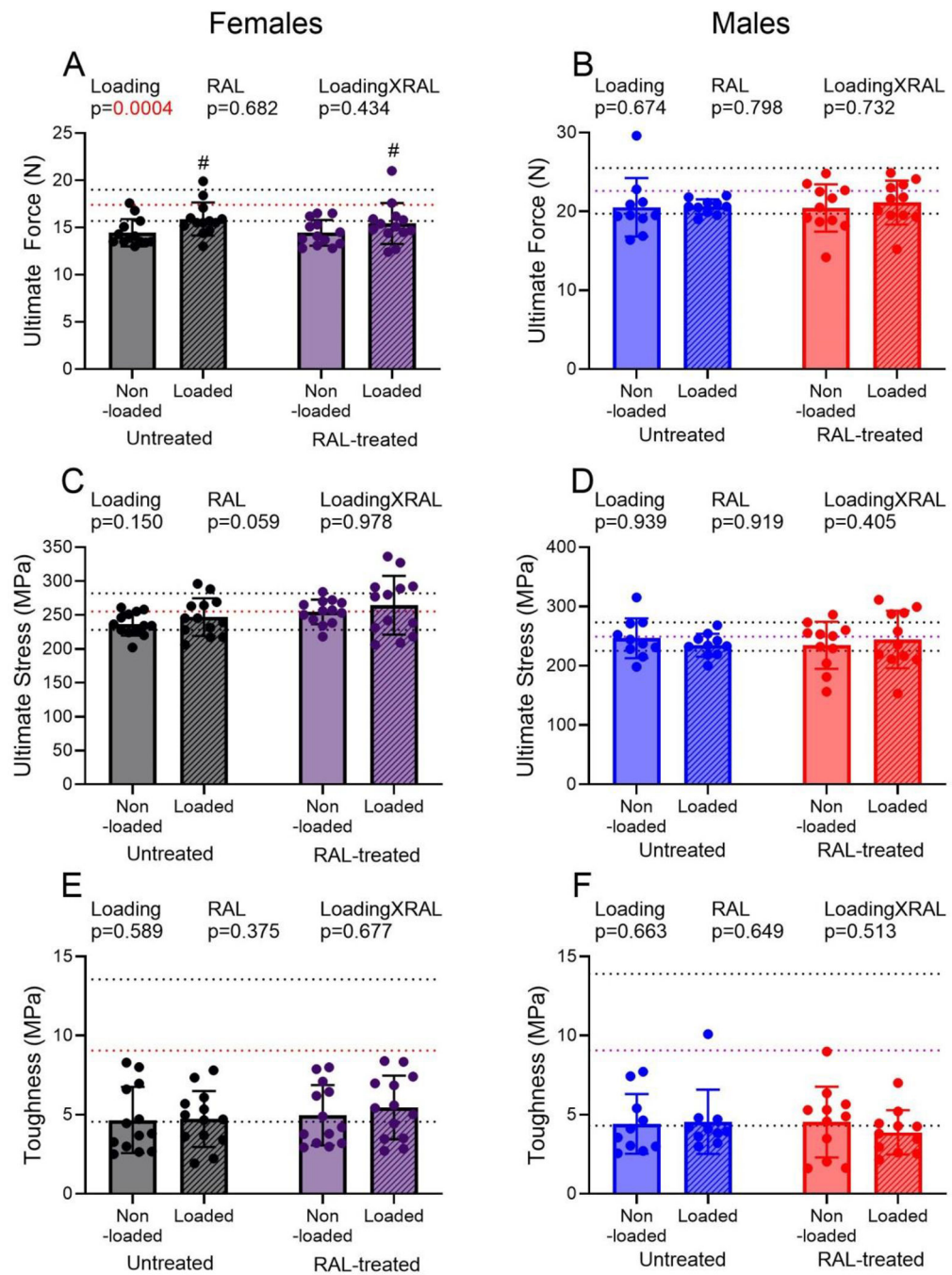


Figure 2: Ultimate force of female (A) and male (B) OI mice, ultimate stress of female (C) and male (D) mice, and toughness of female (E) and male (F) OI mice. # indicates difference with loading. Dotted lines on graphs indicate the average and standard deviations of wild-type non-loaded untreated mice. Two way ANOVA p values reported above graphs.

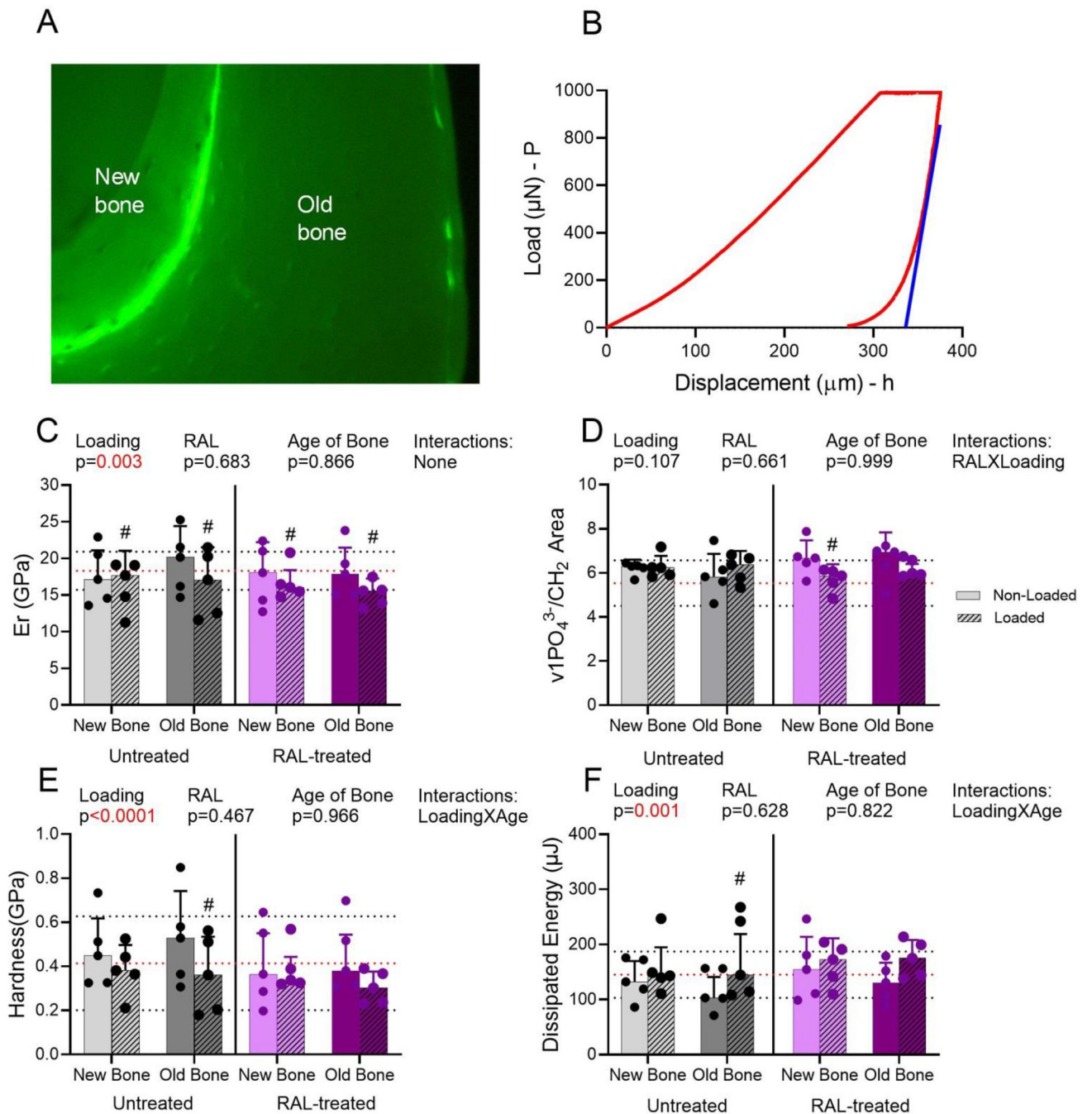


Figure 3: Raman and nanoindentation measurements of tibiae. Example image of determination of new versus old bone (A), example nanoindentation curve (B), modulus (E_r) (C), $\nu 1\text{PO}_4^{3-}/\text{CH}_2$ (D), hardness (E), and dissipated energy (F). # indicates difference with loading. Lined bars indicate loaded bone. Dotted lines on graphs indicate the average and standard deviations of old bone in wild-type non-loaded untreated mice.

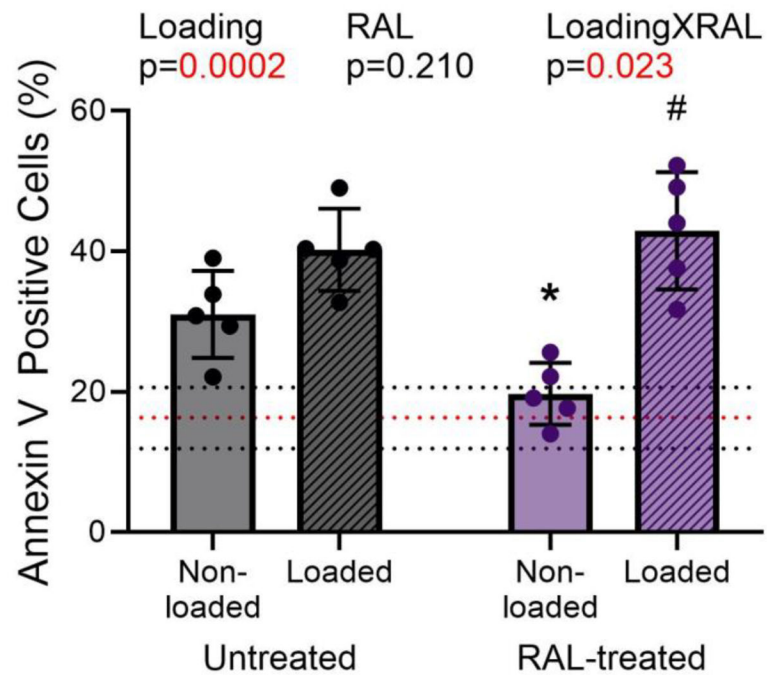


Figure 4: Osteocyte apoptosis in OI female mice as measured by annexin V from IHC. # indicates difference with loading and * indicates difference with RAL treatment. Dotted lines on graphs indicate the average (red) and standard deviations (black) of wild-type non-loaded untreated mice.

Table 1: MicroCT measures of female and male OI mice and p values from two-way ANOVA.

Property	Loading	Female OI Untreated (n=13)	Female OI RAL-Treated (n=13)	Male OI Untreated (n=10)	Male OI RAL-Treated (n=11)	Loading	RAL	Inter.
<i>Cortical bone</i>								
Total area (mm ²)	N	1.03±0.07	1.03±0.06	1.30±0.07	1.33±0.11	Female	< 0.0001	0.553 0.447
	L	1.11±0.08	1.09±0.05	1.33±0.06	1.37±0.07	Male	0.015	0.282 0.596
Marrow area (mm ²)	N	0.354±0.050	0.341±0.023	0.457±0.037	0.449±0.054	Female	< 0.0001	0.130 0.115
	L	0.396±0.055	0.363±0.022	0.466±0.050	0.457±0.046	Male	0.321	0.666 0.962
Imax (mm ⁴)	N	0.175±0.027	0.161±0.016	0.258±0.022	0.263±0.045	Female	0.007	0.138 0.968
	L	0.186±0.035	0.173±0.016	0.267±0.020	0.287±0.029	Male	0.030	0.309 0.330
<i>Trabecular bone</i>								
BV/TV (%)	N	8.9±1.4	10.7±1.7	17.0±3.0	21.7±3.4	Female	0.001	0.001 0.477
	L	9.7±1.5	11.9±1.1	19.4±2.0	23.3±3.5	Male	0.002	0.003 0.467
Trabecular thickness (mm)	N	0.0614±0.0030	0.0617±0.0019	0.0628±0.0035	0.0680±0.0034*	Female	< 0.0001	0.857 0.585
	L	0.0667±0.0033	0.0661±0.0034	0.0684±0.0032#	0.0689±0.0032	Male	0.001	0.028 0.009
Trabecular spacing (mm)	N	0.297±0.050	0.281±0.037	0.193±0.014	0.191±0.013	Female	0.468	0.066 0.011
	L	0.307±0.052	0.263±0.018#*	0.187±0.007	0.186±0.014	Male	0.081	0.613 0.894
Trabecular number (1/mm)	N	1.46±0.26	1.74±0.26	2.69±0.38	3.17±0.36	Female	0.360	0.001 0.380
	L	1.46±0.23	1.81±0.19	2.84±0.29	3.37±0.38	Male	0.015	0.002 0.745

N indicates non-loaded right tibiae and L indicates loaded right tibiae.

indicates differences with loading compared to non-loaded control of same treatment group

* indicates difference with raloxifene in same load group for parameters with significant interaction terms.

Table 2:

Percent change and effect sizes of loaded untreated bones (L), non-loaded RAL-treated bones (R), and loaded RAL-treated bones (L+R) compared to non-loaded untreated bones of the same sex.

Property	Female OI						Male OI					
	% Change			Effect Size			% Change			Effect Size		
	L	R	L+R	L	R	L+R	L	R	L+R	L	R	L+R
<i>Cortical bone</i>												
Total area (mm ²)	7.63	-0.51	5.39	1.02	0.08	0.93	2.53	2.16	5.84	0.50	0.30	1.06
Marrow area (mm ²)	11.9	-3.58	2.51	0.80	0.32	0.23	2.03	-1.67	0.16	0.21	0.17	0.02
Bone area (mm ²)	5.44	1.09	6.89	0.74	0.15	1.07	2.80	4.23	8.93	0.60	0.48	1.48
BA/TA (%)	-2.04	1.43	1.28	0.40	0.33	0.30	0.37	1.95	2.95	0.11	0.46	0.88
Cortical Thickness (mm)	-0.48	0.93	3.16	0.07	0.13	0.48	0.87	3.99	6.52	0.24	0.51	1.22
Imin (mm ⁴)	22.9	4.72	24.3	1.41	0.30	1.76	7.05	9.98	17.7	0.57	0.60	1.28
Imax (mm ⁴)	6.60	-7.80	-1.35	0.37	0.61	0.11	3.69	1.88	11.1	0.45	0.14	1.11
Ct.TMD	-0.12	1.41	2.10	0.05	0.72	0.92	1.10	0.36	0.02	0.71	0.17	0.01
<i>Trabecular bone</i>												
BV/TV (%)	9.08	20.4	33.8	0.57	1.17	2.40	14.5	27.6	37.1	0.96	1.45	1.92
Trabecular thickness (mm)	8.50	0.40	7.59	1.66	0.10	1.44	8.98	8.27	9.70	1.69	1.51	1.82
Trabecular spacing (mm)	3.43	-5.34	-11.3	0.20	0.36	0.89	-3.13	-1.43	-4.07	0.54	0.20	0.56
Trabecular number (1/mm)	0.24	19.3	24.1	0.01	1.08	1.53	5.68	17.9	25.2	0.45	1.30	1.78
<i>Bulk mechanics</i>												
Yield force (N)	9.26	0.90	10.4	0.58	0.07	0.72	-15.0	-9.62	-6.55	0.73	0.54	0.34
Ultimate force (N)	10.1	0.20	6.73	0.91	0.02	0.53	0.37	-0.43	2.88	0.03	0.03	0.18
Yield displacement (µm)	-3.11	1.82	12.2	0.28	0.18	0.69	-14.1	-18.4	-11.9	0.89	1.34	1.00
Post-yield displacement (µm)	0.36	19.2	10.9	0.00	0.22	0.13	60.5	37.8	12.4	0.48	0.40	0.16
Total displacement (µm)	-1.68	8.98	11.7	0.05	0.26	0.38	9.81	-0.42	-4.13	0.30	0.02	0.17
Stiffness (N/mm)	12.8	-0.61	0.45	0.70	0.05	0.02	1.23	16.6	7.08	0.07	0.66	0.43
Yield work (mJ)	4.23	2.61	21.3	0.22	0.15	0.89	-22.9	-24.6	-14.8	0.85	1.05	0.57
Post-yield work (mJ)	6.84	5.13	14.3	0.09	0.07	0.18	40.2	29.5	5.24	0.39	0.34	0.07
Total work (mJ)	5.68	4.01	17.4	0.15	0.10	0.41	6.84	0.89	-5.36	0.15	0.02	0.13
<i>Material properties</i>												
Yield stress (MPa)	3.08	9.15	15.8	0.29	0.96	1.08	-19.8	-13.7	-9.94	1.12	0.88	0.51
Ultimate stress (MPa)	4.32	7.64	11.7	0.44	1.03	0.84	-4.88	-4.81	-0.78	0.44	0.32	0.05
Yield strain (me)	-1.04	-2.79	9.21	0.09	0.27	0.50	-12.5	-14.8	-12.7	0.73	0.93	0.86
Total strain (me)	0.79	3.86	8.66	0.02	0.12	0.30	9.64	3.94	-7.04	0.32	0.12	0.31
Modulus (GPa)	4.44	12.2	8.67	0.27	0.91	0.33	-5.07	7.81	6.68	0.30	0.31	0.28
Resilience (MPa)	0.64	6.15	23.7	0.04	0.38	0.97	-26.4	-25.4	-20.3	0.98	1.03	0.79
Toughness (MPa)	1.37	6.54	17.1	0.03	0.15	0.39	2.93	2.57	-12.1	0.07	0.05	0.32

Table 3:

Mechanical properties of female and male OI mice and p values from two-way ANOVA.

Property	Loading	Female OI Untreated (n=13)	Female OI RAL-Treated (n=13)	Male OI Untreated (n=10)	Male OI RAL-Treated (n=11)	Loading	RAL	Inter.
<i>Bulk mechanics</i>								
Yield force (N)	N	13.0±1.6	13.1±1.5	18.9±3.8	17.1±2.8	Female	0.002	0.857
	L	14.2±2.4	14.3±2.1	16.0±3.9	17.6±3.4	Male	0.325	0.920
Yield displacement (µm)	N	244±22	248±27	245±29	200±38*	Female	0.371	0.058
	L	236±31	274±57	211±47#	216±30	Male	0.316	0.146
Yield work (mJ)	N	1.76±0.27	1.80±0.34	2.51±0.61	1.89±0.56	Female	0.081	0.119
	L	1.83±0.39	2.13±0.53	1.93±0.73	2.14±0.69	Male	0.412	0.332
<i>Material Properties</i>								
Yield stress (MPa)	N	211±16	231±24	226±36	195±35	Female	0.144	0.014
	L	218±27	245±41	182±44	204±50	Male	0.174	0.731
Resilience (MPa)	N	2.02±0.23	2.15±0.40	2.35±0.60	1.75±0.55	Female	0.152	0.026
	L	2.03±0.39	2.50±0.66	1.73±0.66#	1.87±0.60	Male	0.151	0.285

N indicates non-loaded right tibiae and L indicates loaded right tibiae.

indicates differences with loading compared to non-loaded control of same treatment group

* indicates difference with raloxifene in same load group for parameters with significant interaction terms.